Raman spectroscopy study of heat-treated and boron-doped double wall carbon nanotubes

F. Villalpando-Paez,[1] H. Son,[2] S. G. Chou,[3] Ge. G. Samsonidze,[2] Y. A. Kim,[4] H. Muramatsu,[4] T. Hayashi,[4] M. Endo,[4] M. Terrones,[5] and M. S. Dresselhaus[2,6]

[1]*Department of Materials Science and Engineering, Massachusetts Institute of Technology, Cambridge, Massachusetts 02139-4307, USA*

[2]*Department of Electrical Engineering and Computer Science, Massachusetts Institute of Technology, Cambridge, Massachusetts 02139-4307, USA*

[3]*Physics Division, National Institute of Standards and Technology, Gaithersburg, Maryland 20899-1070, USA*

[4]*Faculty of Engineering, Shinshu University, 4-17-1 Wakasato, Nagano-shi 380-8553, Japan*

[5]*Advanced Materials Department, IPICYT, San Luis Potosi, 78216, Mexico*

[6]*Department of Physics, Massachusetts Institute of Technology, Cambridge, Massachusetts 02139-4307, USA*

(Received 28 February 2009; revised manuscript received 10 May 2009; published 16 July 2009)

We performed Raman spectroscopy experiments on undoped and boron-doped double walled carbon nanotubes (DWNTs) that exhibit the "coalescence inducing mode" as these DWNTs are heat treated to temperatures between 1200 °C and 2000 °C. The fact that boron doping promotes DWNT coalescence at lower temperatures allowed us to study in greater detail the behavior of first- and second-order Raman modes as a function of temperature with regard to the coalescence process. Furthermore, by using various excitation laser energies we probed DWNTs with different metallic (M) and semiconducting (S) inner and outer tubes. We find that regardless of their M and S configurations, the smaller diameter nanotubes disappear at a faster rate than their larger diameter counterparts as the heat treatment temperature is increased. We also observe that the frequency of the G band is mostly determined by the diameter of the semiconducting layer of those DWNTs that are in resonance with the laser excitation energy. Finally, we explain the contributions to the G′ band from the inner and outer layers of a DWNT.

DOI: 10.1103/PhysRevB.80.035419 PACS number(s): 63.22.−m, 81.07.De

I. INTRODUCTION

The mechanical and electronic properties of carbon nanotubes are not only highly dependent on nanotube diameter and chirality, but also on the number of concentric layers.[1] Adding layers to a single wall nanotube gives rise to charge transfer effects[2] and also enhances its chemical, mechanical, and thermal stability.[3] Since double wall carbon nanotubes (DWNTs) can possess desirable electrical properties characteristic of single wall carbon nanotubes (SWNTs) while being more mechanically robust, they are good candidates for building blocks in electronic devices,[4] where relatively large amounts of energy need to be transferred without compromising the lifetime of the device. In this context, besides controlling the length and diameter of carbon nanotubes, researchers are now making an effort to control the number of layers and numerous attempts have been made to fabricate high quality DWNTs.[5–10]

In this work we study a DWNT material where previous Raman spectroscopy studies have revealed the presence of the "coalescence inducing mode" (CIM).[11] The CIM has been identified as a novel resonant Raman mode related to the vibration of one-dimensional carbon chains (3–5 atoms long) that are created in DWNTs by heat treatment. The appearance of these linear carbon chains by Raman spectroscopy was correlated with the coalescence of the DWNTs, as observed by high resolution TEM measurements.[11] In this early study,[11] Raman spectra for these DWNTs were only studied at 2.33 eV.

Herein we present a detailed study of the comparison in behavior between boron-doped and undoped DWNT samples with regard to heat treatment to various temperatures, in general, and with regard to further exploration of what Raman spectroscopy tells us about the role of boron in the coalescence process of DWNTs. Special emphasis is given to whether the inner and outer walls are metallic (M) or semiconducting (S) and comparisons are also made to recent studies of DWNTs carried out at the individual isolated DWNT level.[12] In Sec. II experimental procedures are summarized, while Sec. III is devoted to the results and discussion of these results. In Sec. III A an overview of the Raman studies in these DWNTs is presented while in Secs. III B–III E more detailed results are presented for RBM, D band, G band and G′ band Raman spectra, respectively. Finally, Sec. IV presents a summary and concluding remarks relevant to our findings.

II. EXPERIMENTAL PROCEDURES

We used a catalytic chemical vapor deposition (CCVD) method to synthesize the double walled carbon nanotubes used in this study. As reported elsewhere,[5,13] the buckypaper made with the resulting DWNTs is extremely flexible and macroscopic, and its high purity relative to residual catalyst particles has been confirmed by diamagnetic susceptibility experiments. Its purity relative to SWNTs (single wall carbon nanotubes) has been probed by Raman spectroscopy.[14] In order to dope the DWNTs with boron and to study the effect of boron doping on DWNT coalescence, elemental boron was mixed (0.05 wt %) with the highly purified DWNTs and thermally annealed at various temperatures (T_{htt}) between 1000 and 2000 °C for 30 minutes in a high purity argon atmosphere. Since we dope DWNTs with elemental boron and all our heat treatments are performed in an argon

atmosphere, we only expect to have partial substitution reactions where only a small fraction of carbon atoms in the CNT lattice are substituted by B atoms. Two batches of samples were fabricated using the same synthesis method but on different experimental runs. The first batch contains three samples that we used for undoped experiments (Pristine, $T_{htt}=1500$, $T_{htt}=2000$ °C) and the second batch contains nine samples that we used for B-doping experiments (Pristine, $T_{htt}=1200$, $T_{htt}=1300$, $T_{htt}=1400$, $T_{htt}=1500$, $T_{htt}=1600$, $T_{htt}=1700$, $T_{htt}=1800$, $T_{htt}=2000$ °C). In this work the word "Pristine" indicates no boron doping and no heat treatment. Two different pristine samples were used in this work, neither of which have been heat treated nor boron doped.

Resonance Raman spectra with three different excitation laser energies E_{laser} were taken on the macroscopic mats of the buckypaper described above. Every Raman measurement was conducted at room temperature and the laser power levels were kept below 0.5 mW to avoid excessive heating. A 100× objective lens was used to focus the laser beam on a spot within a 1 μm diameter region and the acquisition times were varied from 5 seconds to 1 minute depending on how strong the Raman signal was. Scattered light was collected through the 100× objective using a backscattering geometry. An Ar^+ ion laser was used to generate $E_{laser}=2.41$ eV, a dye laser containing Rhodamine 6 G dye was pumped by an Ar^+ ion laser to generate $E_{laser}=1.92$ eV, and a Kr^+ ion laser generated $E_{laser}=1.58$ eV. A thermoelectrically cooled Si charge coupled device (CCD) detector operated at −75 °C was used to collect the spectra. Every spectrum was normalized to the intensity of the *G* band and line shape analyses were performed using linear baselines and Lorentzian functions.

III. RESULTS AND DISCUSSION

A. Diameter (d_t) distribution and metallic/semiconducting nature of the resonantly excited layers of DWNTs

In this work, special emphasis was given to the fact that DWNTs can consist of any of the four S@S, S@M, M@S, or M@M configurations, where S@M denotes, for example, a semiconducting (*S*) inner tube within a metallic (*M*) outer tube. Figure 1 shows a theoretical Kataura plot based on the extended tight-binding (ETB) model.[15,16] The laser energies marked on this figure with horizontal lines were chosen to excite different configurations of DWNTs. The shaded regions indicate the diameter distribution of the inner and outer tubes in our DWNT samples.[5,13] Such a Kataura plot, based on prior studies on SWNTs, is accurate enough for the qualitative identification of the (n,m) for small diameter tubes within DWNTs.

By comparing the information provided by the theoretical Kataura plot,[15,17] with our experimental results, we can see that the inner tubes that are in resonance with $E_{laser}=2.41$ eV are *M* tubes with E_{11}^M transitions,[18] while most of the outer tubes that are in resonance with $E_{laser}=2.41$ eV are *S* tubes with E_{33}^S transitions. The corresponding tube diameters d_t that are expected to be in resonance with $E_{laser}=2.41$ eV are 0.87 nm and 1.4 nm, based on the relation $\omega_{RBM}=218.3/d_t+15.9$,[11] where ω_{RBM} is in units of cm^{-1}.

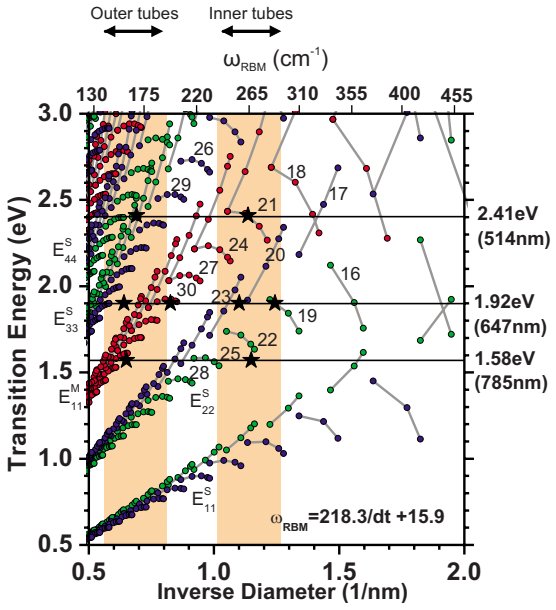

FIG. 1. (Color online) Kataura plot used to determine the metallic or semiconducting nature of the inner and outer tubes of DWNTs in resonance with the laser energies (horizontal lines) used in this study. The relevant $2n+m$ families are marked. Each star on the plot represents a Raman frequency where the RBM intensity is strong. The Kataura plot is calculated within the ETB framework[15] including the many-body corrections fitted to the RRS data from SDS-wrapped HiPCO SWNTs.[17]

On the other hand, if the sample is excited with $E_{laser}=1.58$ eV, the nanotubes that are in resonance are those whose inner (outer) tubes are S (M) with d_t around 0.82 nm (1.56 nm) for $E_{laser}=1.58$ eV. However, the actual inner (outer) tube configurations present in the sample include all four of the possibilities mentioned above. Therefore, it is important to keep in mind that the inner S tubes that are in resonance with a given laser energy may also have outer M or S layers that may be in resonance with the same laser line, but with a much higher probability that the outer tube forming a given DWNT will not be in resonance with that E_{laser}. Moreover, likewise for an inner resonant M tube, its outer tube can be an S or M tube that in general will not be in resonance with the same E_{laser} as the inner tube. Our Raman experiments were performed on bundled samples. It is only by carrying out systematic studies at the individual DWNT level using multiple laser lines that the explicit correlation between the inner and outer tubes of the M@S, S@M, S@S and M@M configurations can be studied in detail.[12]

The (n,m) integers that define the particular structure of a carbon nanotube have been assigned to each nanotube group present in our pristine DWNT (undoped and without heat treatment) sample by relating the measured ω_{RBM} to the theoretical Kataura plot (see Fig. 1). Our (n,m) assignments for the strongest RBM peaks [(8,5) tubes for $E_{laser}=2.41$ eV and (11,0) tubes for $E_{laser}=1.58$ eV] are in agreement with previous Raman characterization studies performed on the same kind of DWNT sample by Souza Filho *et al.*[19] We observed that most of the inner nanotubes present in the DWNT samples when using $E_{laser}=2.41$ eV and $E_{laser}=1.58$ eV, re-

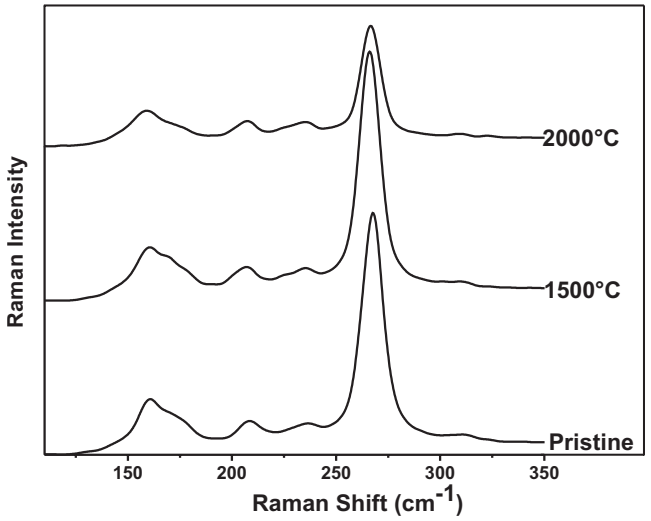

FIG. 2. The RBM region of the Raman spectra of undoped DWNTs taken with $E_{laser}=1.58$ eV. The relatively high intensity of the RBM signal at $T_{htt}=2000$ °C confirms that undoped DWNTs are able to withstand high T_{htt} without suffering substantial structural damage.

spectively, belong to the families $p=21$ containing the (8,5) tube and $p=22$ containing the (11,0) tube, where $p=2n+m$. If we excite the sample with $E_{laser}=1.92$ eV we observe seven RBM peaks corresponding to DWNT layers with diameters that vary from 0.8 to 1.6 nm where the inner tubes are likely to be (7,6) and (7,5) tubes with $d_t \approx 0.93$ nm and $d_t \approx 0.80$ nm, respectively.

B. Radial breathing mode as a function of T_{htt}

1. Undoped DWNT samples

When undoped, our DWNT sample shows exceptionally good structural stability up to high T_{htt} (2000 °C). The Raman intensities (Integrated area of a feature normalized to the integrated area of the G band) of the RBM features for these undoped tubes decrease with increasing T_{htt} (approx. a 50% decrease in intensity when going from the pristine sample to the one for $T_{htt}=2000$ °C) but these Raman intensities remain relatively high even at $T_{htt}=2000$ °C (see Fig. 2). The structural stability at high T_{htt} of similar undoped DWNT samples has also been confirmed by previous high-resolution transmission electron microscopy (HRTEM) and Raman studies.[3]

For Raman spectra taken at $E_{laser}=1.58$ eV,[20] the strongest RBM features correspond to inner tubes (in resonance with E_{22}^S) that have a $d_t \approx 0.88$ nm and to outer tubes (in resonance with E_{11}^M) that have a $d_t \approx 1.55$ nm. Previous HRTEM studies on this kind of DWNT bundled samples[11] have reported an intertube spacing of ~0.34 nm. Considering an intertube spacing of 0.34 ± 0.01 nm between the inner and outer tubes of DWNTs, it is possible that we are exciting the inner and outer layers of the same DWNT because 1.55 nm−0.88 nm=0.67 nm, consistent with an intertube separation of 0.34 nm. This inner semiconducting tube could also be paired up with either an M or S outer tube with a $d_t \approx 1.56$ nm, and this outer tube might be in resonance with $E_{laser}=1.58$ eV or most likely would be outside the resonant window (equivalent to fixing a value or range of values for the outer tube diameter and moving vertically along the Kataura plot in Fig. 1 to find other tubes that are present in the sample but not in resonance with the $E_{laser}=1.58$ eV).

RBM measurements with $E_{laser}=1.58$ eV reveal that there are also tubes with diameters ranging from ~1.0 to ~1.37 nm that also remain intact at temperatures as high as $T_{htt}=2000$ °C. Measurements with $E_{laser}=2.41$ eV gives similar results, confirming the great thermal stability of the undoped DWNTs in an inert atmosphere. These results are in good agreement with measurements at $E_{laser}=2.33$ eV in Ref. 11.

2. Boron doped DWNT samples

Figure 3(a) depicts the RBM region of the spectra (using $E_{laser}=1.58$ eV) from samples that were heat treated at various temperatures in the presence of elemental boron. When compared to the pristine (undoped and not heat treated) samples, the boron-doped DWNT samples start showing structural disorder at much lower T_{htt} than their undoped counterparts. We show in this section that this effect is also found at the other E_{laser} values that were investigated. Also, the behavior of the RBM Raman intensities as a function of T_{htt} (I_{RBM}) in Fig. 3(a), suggests that the smaller d_t (S) tubes disintegrate at a faster rate than their large diameter (M) counterparts. Other weaker RBM features [follow the circles and triangles in Fig. 3(b)] corresponding to tubes with $1.0 < d_t < 1.37$ nm, show RBM intensities that become undetectably small at $T_{htt}=1400$ °C.

Figure 3(b) shows that the most prominent RBM features (e.g., ~267 and ~159 cm^{-1}) correspond to inner tubes (with E_{22}^S in resonance with $E_{laser}=1.58$ eV) that have $d_t \sim 0.88$ nm and to outer tubes (with E_{11}^M in resonance with $E_{laser}=1.58$ eV) that have $d_t \sim 1.55$ nm. As discussed above for the undoped samples, it is possible that some inner semiconducting (S) and outer metallic (M) tubes might belong to the same DWNT, both being in resonance with $E_{laser}=1.58$ eV and having an interlayer distance of ~0.34 nm. At $T_{htt} \geqslant 1700$ °C, the boron-doped samples showed no RBM signal, thus indicating that the DWNTs were destroyed and that their carbon atoms either formed other carbon-based structures or left the system.

It is reasonable to expect that boron doping and heat treatment might affect M and S tubes in different ways. In order to investigate these differences, we switched the laser excitation energy to $E_{laser}=2.41$ eV (see Fig. 1) and excited M inner walls and S outer walls that may or may not correspond to the same DWNTs. Figure 3(c) shows the RBM region of the spectra thus obtained at 2.41 eV as a function of increasing T_{htt} for the boron-doped samples. The same general behavior as depicted in Fig. 3(a) is also observed in this case as T_{htt} increases, the small diameter tubes corresponding to inner tubes of the DWNTs [for example, with family $p=21$, (8,5) for $E_{laser}=2.41$ eV] disappear at a faster rate than their large diameter counterparts, especially for $1400 < T_{htt} < 1600$ °C. Independent of whether the tubes are M or S, we also observe that the intensity of the RBM first increases

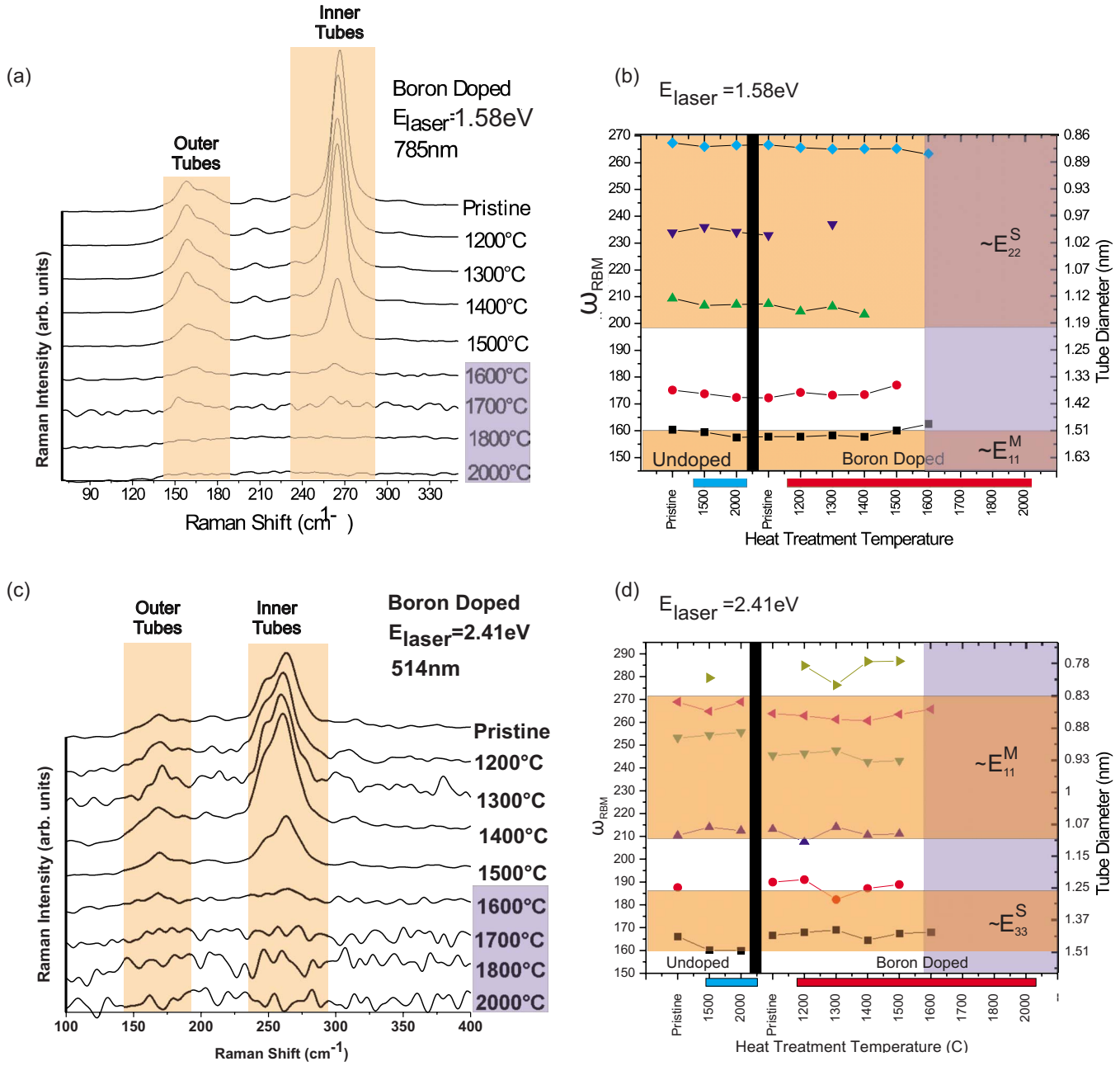

FIG. 3. (Color online) The RBM region of the Raman spectra of boron-doped DWNTs taken with (a) $E_{laser}=1.58$ eV and (c) $E_{laser}=2.41$ eV for samples exposed to various heat treatment temperatures. (b) and (d) show the frequency of the various observed RBM features (ω_{RBM}) and their corresponding tube diameters (d_t) as a function of heat treatment temperature (°C) for both undoped and boron-doped DWNT samples. The shaded regions in (b) and (d) mark the corresponding metallic or semiconducting nature of the nanotubes according to their location on the Kataura plot shown in Fig. 1. Note that the RBM signal becomes very weak for $T_{htt}>1600$ °C (blue shaded region) indicating that most of the DWNTs in the sample have, as has been previously observed using HRTEM,[11] either coalesced or become a mixture of complex tubular structures and of more disordered carbon.

with T_{htt} as defects are annealed (Pristine to $T_{htt}=1200$ °C), it then reaches a maximum which coincides with the appearance of the CIM (Ref. 11) ($T_{htt}=1300$ and 1400 °C), and then the intensity decreases sharply as the tubes start to coalesce or to transform to other carbon forms such as noncylindrical structures ($T_{htt}\geq 1500$ °C).

Regardless of whether they are metallic or semiconducting [follow squares and rotated triangles in Fig. 3(d)], when subjected to heat treatment, the inner tubes always tend to disappear at T_{htt} between 1400–1600 °C and the outer tubes disintegrate as 1600 °C is reached. Therefore, from the RBM data taken with two laser lines (1.58 and 2.41 eV) that excite the (M inner, S outer) and (S inner, M outer) tube configurations, respectively, we conclude that the metallic or semiconducting nature of the outer layers of a DWNT does not change the temperature at which the coalescence process starts. However, one must keep in mind that the T_{htt} steps used for our set of heat treated samples might be too large to

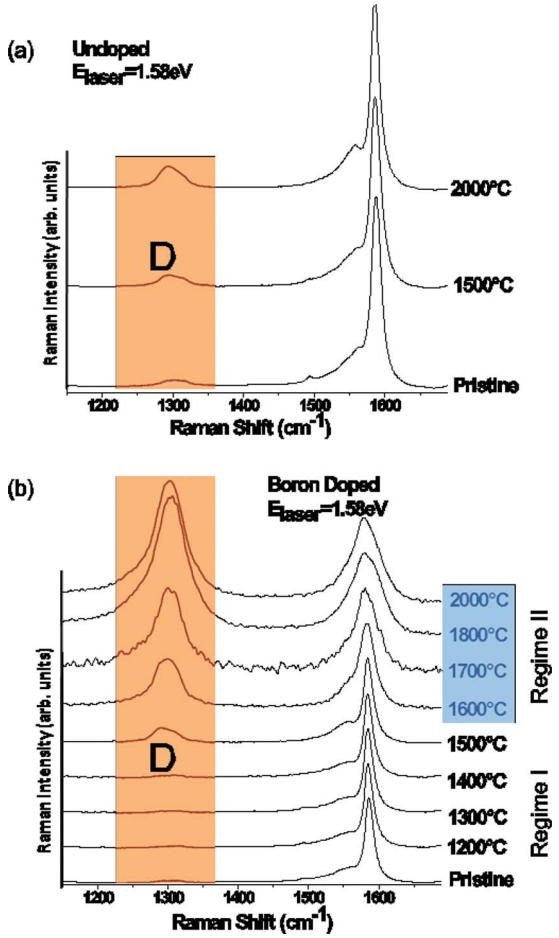

FIG. 4. (Color online) Raman spectra showing the D band (shaded region) of undoped (a) and boron-doped (b) DWNTs taken with $E_{laser}=1.58$ eV.

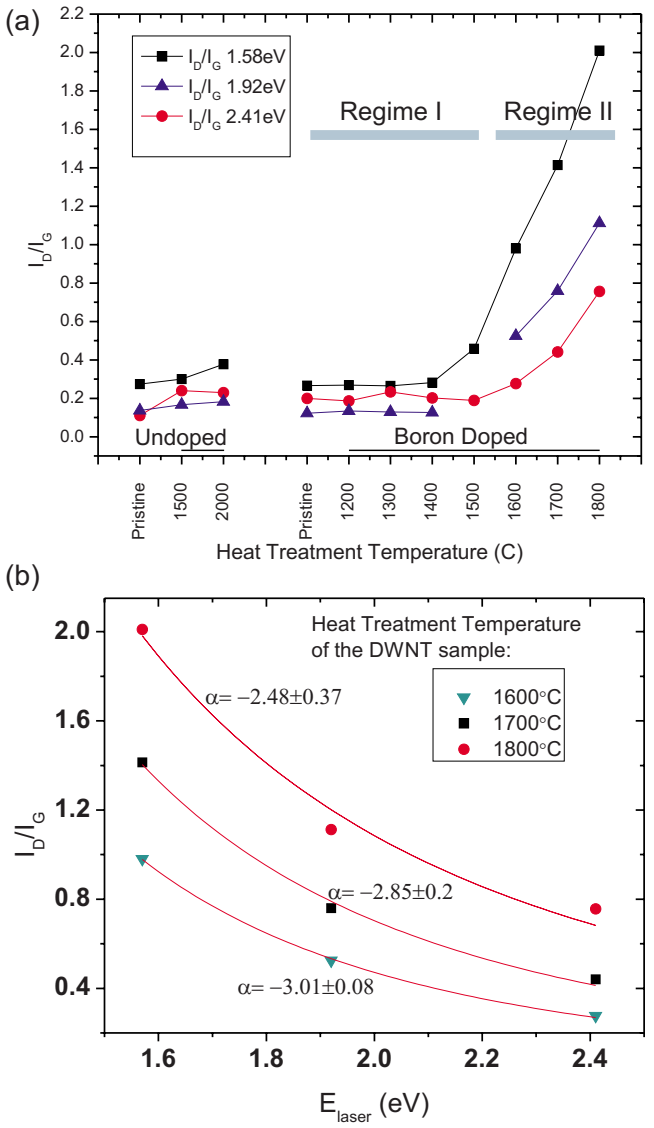

FIG. 5. (Color online) (a) I_D/I_G ratio values of the D-band feature as a function of heat treatment temperature (°C) for undoped and boron-doped samples for various values of E_{laser}. The I_D/I_G values are calculated by integrating the area under the D-band region and dividing it by the area under the G-band region without the use of fitted baselines. (b) The laser energy dependence of I_D/I_G for DWNT boron-doped samples with different heat treatment temperatures. The solid lines show the best E_{11}^M fit curves where c is a constant and α gives the power-law dependence discussed below.

detect small differences in the coalescence onset temperatures between DWNTs with different metalicities.

C. D band as a function of T_{htt} and boron doping

As for the case of the RBM feature, the behavior of the disorder-induced D band is very different for the undoped and the boron-doped DWNT samples, for various heat treatments, as discussed below.

1. Undoped DWNT samples

The D band intensity is very weak ($I_D/I_G=0.1$ at 2.41 eV and 0.29 at 1.58 eV) in the Raman spectra from the pristine (undoped) samples that did not receive any heat treatment. This observation, along with previous scanning electron microscopy (SEM), TEM, and magnetic susceptibility experiments,[5] corroborates the good quality and high purity of our DWNT buckypaper samples.

The pure (undoped) DWNT samples in Fig. 4(a) show only a weak increase in the D-band intensity with increasing T_{htt}. The low D band intensity at $T_{htt}=2000$ °C ($I_D/I_G=0.22$ at 2.41 eV and 0.39 at 1.58 eV) is consistent with the RBM results indicating that only a small portion of the DWNTs in the sample has been transformed into non-nanotube carbon-based material. The low D band intensity is also consistent with previous HRTEM studies[11] concluding that in the absence of elemental boron, the structure of the DWNTs remains relatively undamaged, even at $T_{htt}=2000$ °C. Figure 5(a) shows the I_D/I_G ratio for different E_{laser}, showing that it is best to measure the D band using low E_{laser} values because the D band intensity depends on E_{laser} as E_L^{-3} or E_L^{-4} depending on the type of sample under consideration.[21–24] Thus improved spectral resolution for studying D band properties is achieved when using lower

TABLE I. D-band doublet parameters from undoped and B-doped DWNT samples that were heat treated at $T_{htt}=1500$ °C. The I_D, I_G, I_{DL}, and I_{DH} values correspond to the integrated area of the Lorentzian peaks that were fitted to the D and G band spectral regions after choosing adequate linear baselines (see Fig. 6).

T_{htt} 1500 °C	E_{laser} (eV)	I_D/I_G	I_{DL}/I_{DH}	$FWHM_{DH}$ (cm^{-1})	$FWHM_{DL}$ (cm^{-1})	ω_{DH} (cm^{-1})	ω_{DL} (cm^{-1})
Undoped	1.58	0.30	2.2	22.08	27.45	1312.5	1292.4
B doped	1.58	0.45	1.24	25.6	26.28	1306.8	1288.5
Undoped	2.41	.045	1.15	23.77	29.88	1351.3	1330.4
B doped	2.41	0.18	3.19	21.22	29.7	1350.9	1333.5

E_{laser} values. The results of Fig. 5(a) show that the D band intensity for the undoped samples remains low for all T_{htt} values and all E_{laser} values that were investigated.

2. Boron-doped DWNT samples

Figure 4(b) shows the Raman spectra taken with $E_{laser}=1.58$ eV from boron-doped samples that received heat treatments at various temperatures. As shown by comparison of the D band intensity in Figs. 4(a) and 4(b), the presence of elemental boron during heat treatment enhances the development of structural disorder (and thus the appearance of a more intense D band) at lower T_{htt} (starting at $T_{htt}=1500$ °C) when compared to undoped samples.

On the basis of the experimental results shown in Fig. 4(b), the spectral behavior for the boron-doped samples with respect to T_{htt} can be divided into two regimes: regime I corresponds to $T_{htt}\leqslant 1500$ °C where the spectral profile is dominated by DWNTs and regime II corresponds to $T_{htt}>1500$ °C where the spectral profile is consistent with the increasing domination by non-DWNT structures such as noncylindrical tubules, which are seen in the HRTEM measurements previously reported.[11]

It is important to keep in mind that boron addition has two separate effects on DWNTs: it dopes the nanotubes, changing their Fermi level and boron addition also lowers the T_{htt} at which structural disorder starts to occur. Since both effects occur simultaneously as T_{htt} increases, it is difficult to distinguish between them and to quantify their independent contributions.

a. Regime: $T_{htt}\leqslant 1500$ °C. The bottom half of the shaded region in Fig. 4(b) shows the Raman spectra (using $E_{laser}=1.58$ eV) from boron-doped samples that were heat treated at $T_{htt}=1500$ °C and below. The corresponding values of the I_D/I_G intensity ratio of the D band and G band features in this T_{htt} regime are plotted as a function of heat treatment temperature (T_{htt}) in Fig. 5(a). Figures 4(b) and 5(a) show that the I_D/I_G ratio remains low over the whole range of T_{htt} in regime I and no significant changes in ω_D, I_D/I_G, or the full width of half maximum ($FWHM_D$) linewidth are observed. The low D band intensity in this regime indicates that the DWNTs in our sample can withstand T_{htt} below 1500 °C without major structural damage even when doped with boron. The onset of D band intensity occurs between 1400 ($I_D/I_G=0.29$) and 1500 °C ($I_D/I_G=0.45$), in agreement with prior studies at $E_{laser}=2.33$ eV.[11] It is only at $T_{htt}=1500$ °C that a significant D-band feature appears for both the undoped and B-doped samples [see Table I and Figs. 4(a) and 5(b)].

In order to fully characterize a DWNT one needs to know not only the (n,m) indices of its inner and outer tubes but also the relative atomic positions of the constituents of each tube with respect to one another. The layers of a double wall carbon nanotube are weakly coupled in order to minimize the total energy of the system. Therefore, the electronic structure of a DWNT can be interpreted as the addition of two electronic structures coming from each of its constituents with only a weak modification due to interlayer interactions. The asymmetric line shape of our D band suggests that the spectral profile should be fitted with two Lorentzians and the D band has a well-documented diameter dependence,[18] so we assign the origin of the lower frequency component D_L and higher frequency component D_H to the inner and outer layers, respectively. This assignment is justified by the measurements on isolated individual DWNTs which have very weak D bands (too weak for line-shape analysis), but they have strong G′ bands which involves the same phonons as the D band in a double resonance process. The experimental results for the isolated individual DWNTs show only two peaks, both with large intensities with the lower frequency component associated with the inner tube, and the upper frequency associated with the outer tube.[12]

If DWNT coalescence is catalyzed by boron doping and if the inner tubes start disappearing at a lower heat treatment temperature than the outer tubes due to their higher curvature, it would be reasonable to expect the D band intensity of the inner tubes (D_L) to be greater than that of the outer tubes (D_H). The same principle should apply for both undoped and B-doped samples at a given T_{htt} value but the effect would be more pronounced for B-doped samples where the D-band intensities are higher, as can be seen by comparing the D-band spectra for $T_{htt}=1500$ °C (see Table I and Fig. 6).

In order to study the D_H and D_L spectral features we used the samples that were heat treated at 1500 °C because they are the only ones where both the intensities of the D band and the RBM are large enough to allow for adequate line-shape analysis. This means that at $T_{htt}=1500$ °C the D band intensity is large enough for an accurate line-shape analysis to be carried out, while there are still enough DWNTs present in our sample. This is not the case for $T_{htt}=1400$ °C where the RBM intensities are large enough to be analyzed but the D band intensity is too weak to be analyzed in as much detail. This is also not the case for T_{htt}

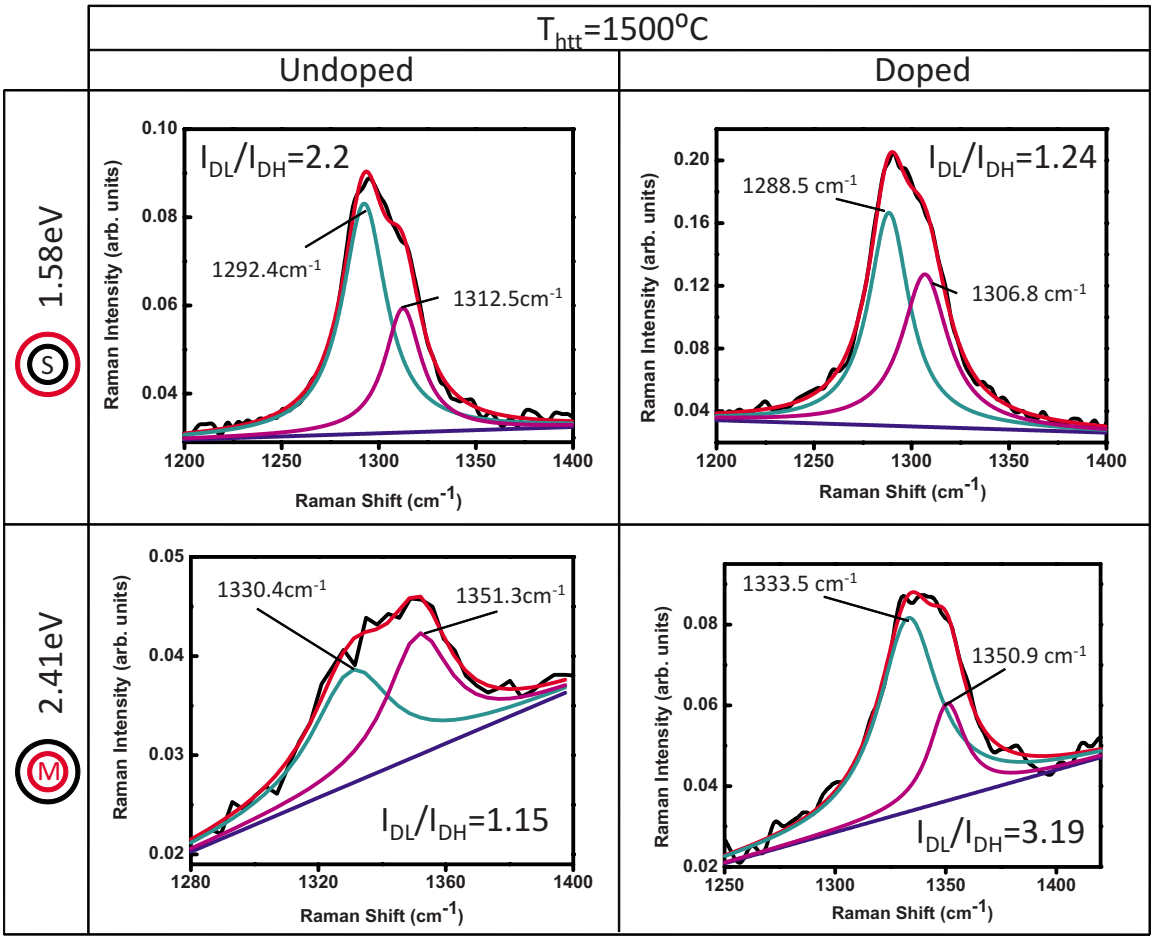

FIG. 6. (Color online) Raman spectra taken with $E_{laser}=1.58$ eV and $E_{laser}=2.41$ eV showing the two Lorentzian peaks used to fit the D band of DWNT samples that were heat treated at $T_{htt}=1500$ °C. For all plots the straight line marks the linear baseline used in the fitting process.

=1600 °C where the D band intensity is large enough to be analyzed, but most of the DWNTs have been destroyed by the coalescence process and the RBM intensity is too weak to analyze.

Figure 6 shows the decomposition of the D-band Raman spectra for a B-doped sample with $T_{htt}=1500$ °C into two Lorentzian components with the low-frequency D band component I_{DL} being more intense than its high-frequency counterpart I_{DH} for $E_{laser}=1.58$ and 2.41 eV and the results are summarized in Table I. The results show that $I_{DL}/I_{DH}>1$ for both undoped and B-doped samples at both values of E_{laser}. However, if we look carefully, we observe that when using 1.58 eV (2.41 eV), the ratio I_{DL}/I_{DH} decreases (increases) with B doping. This complex behavior is a probable indicator that different mechanisms are in play for different DWNT configurations and this complex behavior needs to be researched further preferably at the individual DWNT level.

Those DWNTs with an outer metallic layer (DWNTs excited with 1.58 eV) show a larger overall intensity of the D band (ratio) than those DWNTs (DWNTs excited with 2.41 eV) that have an outer semiconducting layer. Even though the doping effect is subtle and mixed with the E_{laser} dependence of I_D/I_G, the S or M character of the constituent tubes plays a role in the increase of the I_D/I_G ratio because the metallicity (M or S) of the outer tube affects the degree of interaction that the outer layer has with the dopant. A higher degree of interaction of the outer tube with the dopant would imply a faster insertion of foreign atoms into the tube wall and a greater increase in the D band intensity at lower T_{htt}. From a theoretical standpoint this increased interaction of the M outer layer with a dopant is reasonable because the D-band intensity depends on the electron-phonon matrix element and metallic nanotubes have an increased carrier concentration and these carriers are available for increasing the electron-phonon coupling.

b. Regime II: $T_{htt}>1500$ °C. In this T_{htt} regime we observe [in Figs. 4(b), 5(a), and 5(b)] a rapid increase in the I_D/I_G intensity ratio as T_{htt} increases from 1600 to 2000 °C for boron-doped tubes. In addition to the structural destabilization processes that occur for $T_{htt}=1500$ °C and above, boron appears to enter the outer tubes and gives rise to point defect disorder scattering as suggested by structural HRTEM studies.[11] As T_{htt} keeps rising, increased disorder is induced in the sample and various kinds of defects are expected to appear and accumulate. Besides being a probe for the defect density in the sample, the I_D/I_G ratio may also provide a

means to estimate the dopant concentration in the boron-doped DWNT samples. This approach for sample characterization is especially valuable when the doping level is too low to be measured by other commonly used structural characterization techniques such as HRTEM operating in the EELS mode.[25]

The power-law dependence of the I_D/I_G band with varying laser energy is observed in various sp^2 carbon materials and has its origin in a dependence of the electron-photon, electron-phonon, and elastic scattering matrix elements on E_{laser}.[22–24] In the $1600 \leqslant T_{htt} \leqslant 1800$ °C region we observe that decreasing the laser excitation energy increases the overall I_D/I_G ratios. The laser energy dependence of the I_D/I_G ratio for samples with $T_{htt} > 1500$ °C is shown in Fig. 5(b). The figure also contains the best fit of the experimental I_D/I_G data to the functional form cE_L^{α}, where c is a constant and α defines the power-law dependence of I_D/I_G as a function of E_{laser}. The behavior of the D-band Raman intensity as a function of E_{laser} depicted in Fig. 5 is qualitatively consistent with previous experimental and theoretical reports on nanographite[22–24] and SWNTs.[26] In the cited works the dominant effects of increasing the heat treatment temperature were a reduction in the D-band intensity through an increase in crystallite size and a concomitant elimination of defects, as opposed to the heat treatment induced disorder that is studied in our work. However, our experimental trend is similar to previous works regarding the marked increase in the intensity of the I_D/I_G ratios as E_{laser} is decreased.[23] Whereas Fig. 5(b) shows a power-law dependence of the form $I_D/I_G = cE_L^{\alpha}$, where α varies from ~ -2.5 to ~ -3 with increasing T_{htt}, a value of $\alpha = -4$ was reported for systematic studies on nanographite for both experiment[23] and theory.[24] Values for the magnitude of α less than -4 and in a similar range were observed experimentally for graphitic foams where both two-dimensional (2D) and 3D graphite regions are present.[21]

D. G band as a function of T_{htt} and boron doping

The G band contains contributions from all the tubular, graphitic, and sp^2 carbon material in the sample.[18] In particular, for semiconducting tubes, the G^+ feature is generated when carbon atoms vibrate in the axial direction (LO phonon mode) of the nanotube and the G^- feature comes from atoms vibrating along the circumferential direction of the nanotube (TO phonon mode). If the excited nanotube is metallic (semiconducting), the line shape of the G^- is expected to show a Breit-Wigner-Fano (Lorentzian) line shape arising from the conduction electrons interacting with phonons and the Kohn Anomaly causes a large downshift of the LO mode.[27] Charge donors (acceptors) coming from dopants or impurities also modify the Breit-Wigner-Fano line shape and can upshift (downshift) the frequency of the G^+ band.[18] Finally, the configuration of the M or S layers of a DWNT also has an effect on the details of the observed line shape of the G band. Taking these considerations into account, the following trends were observed in the G-band region of the spectra as a function of T_{htt} and boron doping.

1. Undoped DWNT samples

Figure 4(a) shows the G-band region of the Raman spectra of a pristine (no doping and no heat treatment) DWNT sample taken with $E_{laser} = 1.58$ eV. The G^+ feature is relatively sharp and although the inner tubes that are excited by $E_{laser} = 1.58$ eV are predominantly semiconducting, a weak BWF tail appears in the G^- region. We first discuss the G^- feature and then the G^+ feature. The observed BWF line shape of the G^- feature suggests a contribution coming from outer metallic tubes whose E_{11}^M could be in resonance with $E_{laser} = 1.58$ eV. Keep in mind that the inner tubes excited by $E_{laser} = 1.58$ eV may also have outer semiconducting layers that are out of resonance with $E_{laser} = 1.58$ eV. At $T_{htt} = 2000$ °C, the G^- region loses some of its original BWF shape and a sharper G^- feature than the one observed in the nonheat treated sample is noticeable. If we ignore a possible increase in the average d_t due to the high T_{htt}, the observed change towards a more semiconducting line shape at $T_{htt} = 2000$ °C could suggest that the sample's ratio of metallic to semiconducting tubes decreases because metallic tubes might be more sensitive to heat treatment than semiconducting nanotubes and thus more readily destroyed. The change in the metallic/semiconducting ratio is expected to be subtle because, regardless of their metallic or semiconducting nature, undoped tubes can withstand high heat treatment temperatures without showing significant structural damage.

Figure 7(c) shows the dependence of ω_{G+} on T_{htt} for undoped samples using three different laser excitation energies. As can be appreciated from the left-hand side of Fig. 7(c), the undoped DWNT samples did not show significant changes in the frequency of G^+ (FWHM line width of G^+ also remained constant) as T_{htt} was increased. This observation, along with the fact that the G^+ feature remains sharp at all T_{htt}, is yet another confirmation that, in the absence of boron, pure DWNTs are stable under heat treatments to temperatures up to 2000 °C.[11]

So far we have described the behavior of the G band as observed by using $E_{laser} = 1.58$ eV. As previously mentioned in the RBM section, if we switch to $E_{laser} = 2.41$ eV, we excite DWNTs whose inner walls are metallic and outer walls are semiconducting, keeping in mind that the inner M layers in resonance with this laser energy may also be contained inside nonresonant M outer walls. The overall behavior of the G^+ band using $E_{laser} = 2.41$ eV as a function of T_{htt} is similar to its $E_{laser} = 1.58$ eV counterpart, but there is one important difference that should be noted, the ω_{G+} is upshifted by ~ 8 cm^{-1} for all T_{htt} in regime I relative to the data at 1.58 eV [see Fig. 7(c)]. We attribute this offset in ω_{G+} to the change in the excited DWNT configuration from DWNTs with M inner tubes when using $E_{laser} = 2.41$ eV to DWNTs with S inner tubes when using $E_{laser} = 1.58$ eV. Alternatively, we could also expect this upshift to have its origin in the d_t dependence of ω_{G-} for S tubes. According to Paillet,[28] the ω_{G-} for S tubes tends to downshift as d_t decreases. Also, from Raman studies on isolated SWNTs,[18] it is known that S tubes show sharper and more intense G band features than M tubes. In this context, we could be observing how S constituents in our DWNTs dominate the G-band signal and tend to

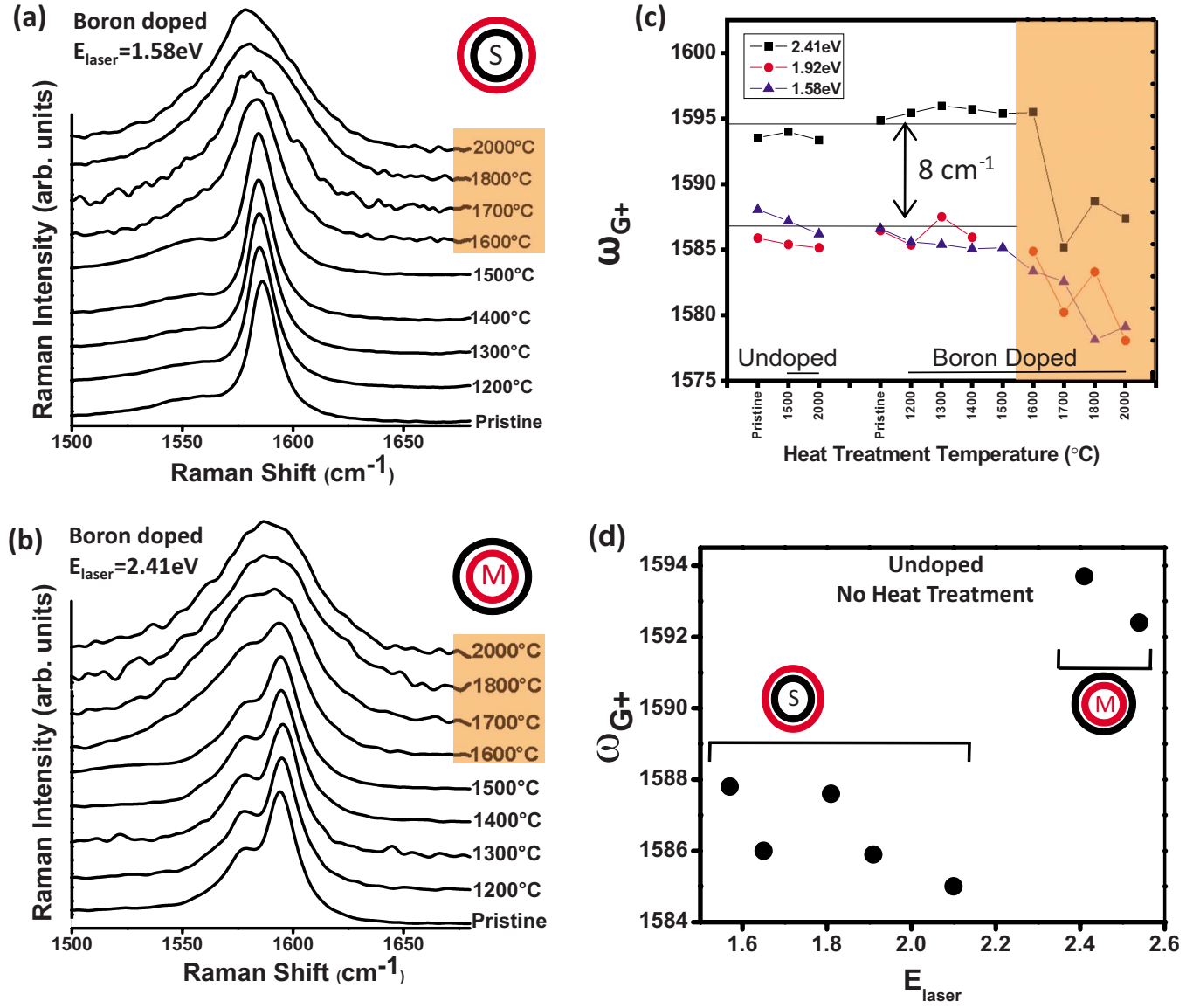

FIG. 7. (Color online) (a) G band region of the Raman spectra of boron-doped DWNTs taken with $E_{laser}=1.58$ eV and taken with (b) $E_{laser}=2.41$ eV. Note the presence of a distinguishable G^- feature for $T_{htt} \leqslant 1500$ °C. (c) Frequency shift of the G^+ band for undoped (left) and boron-doped (right) samples as a function of increasing (T_{htt}). Note that $E_{laser}=2.41$ eV excites tubes whose inner wall is metallic. DWNTs whose inner wall is semiconducting are excited when using $E_{laser}=1.92$ eV (circles) and $E_{laser}=1.58$ eV (triangles). Note the ~ 8 cm^{-1} offset in ω_{G+} between the two DWNT configurations. The shaded region marks the heat treatment temperatures where DWNTs begin disintegrating, thus resulting in disordered carbon sp^2 structures and amorphous carbon. (d) G band frequency as a function of E_{laser} from undoped DWNTs without heat treatment, showing an upshift of ω_{G+} for the M@S configuration relative to the S@M configuration. Our measurements probe the M inner tubes for E_{laser} above 2.3 eV and the S inner tubes for E_{laser} below 2.3 eV.

determine the ω_{G+} since different E_{laser} lines excite S tubes with different d_t values. Figure 7(d) shows the behavior of ω_{G+} as a function of E_{laser} for an undoped DWNT sample that did not receive heat treatment. The two ω_{G+} regimes of behavior may suggest that we are switching from S inner tubes/M outer tubes to M inner tubes/S outer tubes as we increase the laser excitation energy. This explanation of the observed upshift in ω_{G+} which is seen in Fig. 7(d) is consistent with observations on individual, isolated DWNTs where ω_{G+} for M@S configurations is also found to be upshifted with respect to the S@M and S@S configurations.[12]

2. Boron-doped DWNT Samples

The simultaneous effects of boron intercalation between DWNTs, boron incorporation into the nanotube lattice, and heat treatment-induced disorder with increasing T_{htt}, are all reflected in the G-band region of the spectra. We discuss the results in terms of the two regimes of heat treatment temperatures and the results for G^+ and G^-.

a. Regime I: $T_{htt} \leqslant 1500$ °C. In this regime no large shifts in the frequency of the G band are observed as a function of increasing T_{htt} for constant laser energy. However, doping and boron incorporation into the nanotube lattice are ex-

pected to generate large shifts in the frequency of the G band. The lack of a large G band shift in this regime indicates that the boron doping levels generated in regime I are low and that most of the atoms contributing to the Raman signal are due to C-C vibrations.

Nevertheless, if we do a careful line-shape analysis, small G band shifts close to the noise level can be seen to follow the same two trends. First, when outer M tubes and inner S tubes are excited with $E_{laser}=1.92$ eV or 1.58 eV [follow the circles and triangles in Fig. 7(c)], a slight ~ 2 cm^{-1} ω_{G+} downshift is observed for increasing T_{htt}. The observed BWF features at T_{htt} below 1500 °C are generated mainly by outer metallic tubes [see Fig. 7(a)], with $d_t \sim 1.56$ nm [see the squares for the RBM in Fig. 3(b)] which are in resonance with E_{11}^{M} for $E_{laser}=1.58$ eV.

Second, when outer S tubes and inner M tubes are excited with $E_{laser}=2.41$ eV [follow the squares in Fig. 7(c)] we find that, in regime I, an arguably small frequency upshift of the G^+ peak (by ~ 2 cm^{-1}) occurs as T_{htt} reaches 1600 °C. These two opposite shifts of ω_{G+} with increasing T_{htt} suggest that when the outer shell of a DWNT is semiconducting ($E_{laser}=2.41$ V), the dominant effect is that of boron acting as an acceptor, which reduces the C-C distance and upshifts ω_{G+}. On the other hand, when the outside layer is metallic, as for the lower E_{laser} values, boron incorporation into the lattice seems to be the dominant effect because the binding energies of B-C bonds are weaker than those of C-C bonds and a downshift of the G^+ phonon frequency is then expected. This result is consistent with the work of Yang *et al.* on nitrogen and boron-doped coaxial nanotubes,[29] where they observe downshifts in the G^+ band as the boron/carbon fraction was increased in their nanotube samples. Thus the observed dependence of ω_{G+} on T_{htt} is consistent with the coalescence process.

b. Regime II: $T_{htt} > 1500$ °C. The effects of boron doping are magnified in this temperature regime. We observe a significant broadening of the G band [see Figs. 7(a) and 7(b)] that has its origin from two simultaneous phenomena, defects and doping as described below. The destruction of carbon nanotubes at high T_{htt} values (above 1600 °C) gives rise to complex Raman spectra.

For $T_{htt} \geqslant 1600$ °C the sample loses crystallinity as linear carbon chains form and trigger nanotube coalescence. In this process carbon nanotubes are destroyed[11] noncylindrical structures form, and other sp^2 and amorphous carbons start to dominate the G band spectra above $T_{htt}=1600$ °C for all E_{laser} values studied. As T_{htt} rises, the contributions to the Raman spectra from complex and heterogeneous sp^2 carbons become more and more important, broaden the G-band line shape dramatically, and downshift the central frequency. These structural changes are correlated with the appearance of a strong D band at T_{htt} above 1500 °C (see Fig. 5) and have been confirmed by complementary studies using HRTEM.[11]

As stated above, boron doping in this regime plays two roles, forming B-C bonds which lowers ω_G and adding hole carriers which increases ω_G and both effects are seen in the spectra. The broadening is more pronounced for the $E_{laser}=2.41$ eV which is resonant with DWNTs with M@S configuration.

E. G′ band as a function of T_{htt} and boron doping

The G′-band feature has its origin from a two phonon second-order Raman resonance process that is observed at a frequency of approximately twice ω_D. When using $E_{laser}=2.41$ eV, SWNTs with d_t values comparable to that of the outer semiconducting tubes in resonance with this E_{laser} show $\omega_{G'} \approx 2700$ cm^{-1} (Ref. 18) and their G′ band can be fit with a single Lorentzian showing a dispersion of $d\omega_{G'}/dE_{laser}=106$ cm^{-1}/eV. The G′ band of single layer graphene can also be fit with one Lorentzian but if a second layer is added to the system, the electronic bands split, and four peaks are observed in the G′ region.[30] Unlike bilayer graphene, the layers of a DWNT are likely to be incommensurate and weakly coupled so the observed splitting of the G′ in DWNTs could be generated by a phonon softening effect due to the differences in curvature between the inner and outer layers. Since the two diameter distributions of the inner and outer tubes can be further subdivided into metallic and semiconducting categories, in this section we fit the G′ band with four Lorentzians. The independent behavior of each Lorentzian is complex and some overlapping between these categories exists. We however expect the two lower frequency Lorentzians to have their origin coming from inner M or S layers and the two higher frequency Lorentzians to come from outer M or S layers.

1. Undoped DWNT samples

The G′ band region of the undoped DWNT samples reveals four Lorentzian peaks that we have identified as G′1, G′2, G′3, and G′4 [see Fig. 9(a)]. As shown in Fig. 8, the heat treatments (up to $T_{htt}=2000$ °C) of the undoped samples do not have a significant effect on the line shape of the G′ region for all E_{laser} values, indicating again that the DWNTs can withstand high temperatures in the absence of boron. At $T_{htt}=2000$ °C the intensity of the G′ band is slightly decreased, but the RBM features corresponding to the inner diameter tubes are still present and the G′1–G′4 features do not disappear. The spectrum in Fig. 8(a) taken at $E_{laser}=2.41$ eV for the pristine undoped DWNTs has also been fit by other authors with four peaks.[31,32]

If we decrease the laser excitation energy, the overall $FWHM_{G'}$ decreases and the G′1–G′4 features tend to merge into a single peak located at $\omega_{G'}=2582$ cm^{-1} for $E_{laser}=1.58$ eV [see Figs. 8(a)–8(c)]. Also, each G′ component has a different dispersion value (see Table II and, in particular, the G′4 feature shows the closest agreement (within 8%) with the dispersion of SWNTs.

In order to assign the G′1–G′4 features to the inner and/or outer walls of our DWNTs, we can compare their diameter dependence to that of SWNTs $\omega_{G'}=\omega_{G'}^{\circ}+c/d_t$ where $\omega_{G'}^{\circ}$ is the frequency of the G′ feature associated with 2D graphite and c is a constant that accounts for laser excitation energy and type of sample.[33] Interestingly, only the

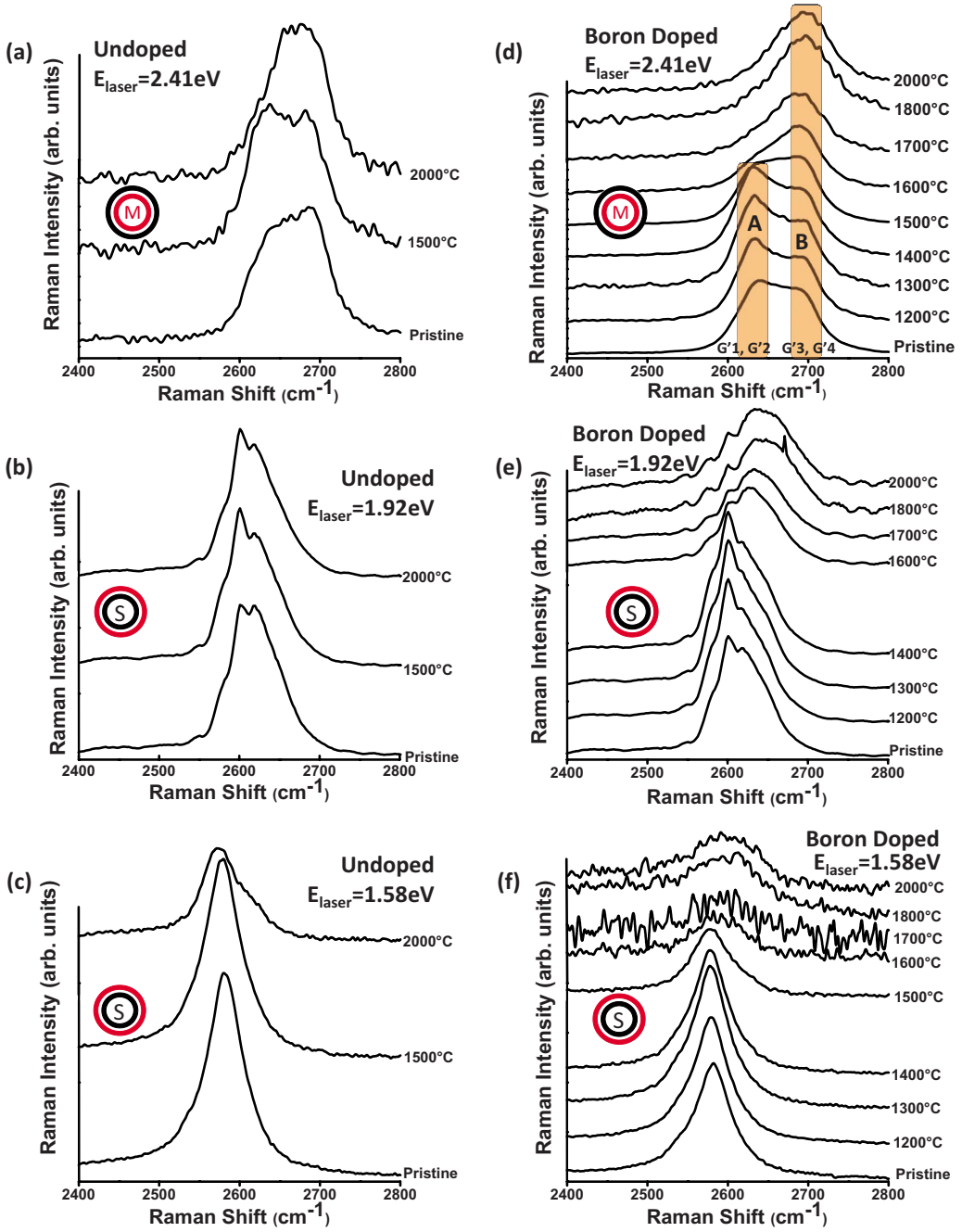

FIG. 8. (Color online) G′ band region of the Raman spectra of undoped and boron-doped DWNT samples for different T_{htt} using (a, d) E_{laser}=2.41 eV, (b, e) E_{laser}=1.92 eV, and (c, f) E_{laser}=1.58 eV. The DWNT schematics mark the metallic or semiconducting nature of the inner tubes that each E_{laser} predominantly excites. The shaded (A) region in (d) marks the low-frequency components of the G′ band (G′1 and G′2) corresponding to the inner diameter tubes. The shaded (B) region for DWNTs corresponds to the G′3 and G′4 features mostly associated with the outer tubes and is observed at all T_{htt}. The predominant excited DWNT configuration for E_{laser}=2.41 eV consists of inner metallic (M) tubes and outer semiconducting (S) tubes.

G′3 feature at $\omega_{G'}$=2663 cm^{-1} [see Fig. 9(a)] shows a reasonable agreement with SWNTs when using E_{laser}=2.41 eV and a d_t=0.88 nm corresponding to the most prominent inner diameter tube in our DWNT sample in resonance at 2.41 eV. When using E_{laser}=1.58 eV the agreement of G′1–G′4 with the $\omega_{G'}$ dependence on d_t for SWNTs is also limited. Therefore, comparisons to SWNT $\omega_{G'}(d_t)$ functions can only be qualitative and a new DWNT $\omega_{G'}(d_t)$ relation has to be developed from experiments on DWNTs with various laser excitation energies. The next section describes how boron doping provided an alternative procedure to investigate the origins of the G′1–G′4 features.

2. Boron-doped DWNT samples

Since boron acts as a catalyst for DWNT coalescence and for the structural destabilization of DWNTs at a lower T_{htt} than in their undoped form, the change in the structure of boron-doped DWNTs as T_{htt} is increased provides further

TABLE II. G′ band dispersion values from pristine (no boron doping and no T_{htt}) and B-doped DWNT samples that were heat treated at $T_{htt}=1400$ °C and $T_{htt}=1600$ °C.

	$\frac{d\omega_{G'}}{dE_{laser}}$ (cm^{-1}/eV)		
Feature	Pristine	$T_{htt}=1400$ °C (Boron doped)	$T_{htt}=1600$ °C (Boron doped)
G′1	86.2	86.4	41.28
G′2	65.04	63.43	47.04
G′3	85.1	73.67	82.4
G′4	98.3	100	85.4

insight into the relationships between the G′1–G′4 features and their identification with the inner and the outer walls of our DWNTs. The G′ band analysis for the boron-doped samples with respect to T_{htt} has also been divided into two regimes: regime I corresponds to $T_{htt}\leqslant 1500$ °C and regime II corresponds to $T_{htt}>1500$ °C.

a. Regime I: $T_{htt}\leqslant 1500$ °C. In the T_{htt} range of regime I, the inner and the outer walls of our DWNTs remain in most cases structurally stable. The frequency, intensity, and dispersion of the G′1–G′4 features show a similar behavior to that of the boron free samples. The dispersion of the G′4 feature (100 cm^{-1}/eV) is again close to the expected 106 cm^{-1}/eV of the G′ band in SWNTs (Ref. 18) and the dispersions of G′1–G′3 are considerably below that value (See Table II column $T_{htt}=1400$ °C).

Figure 8(d) presents the G′ region of the Raman spectra from pristine (no heat treatment and no boron doping) and heat treated boron-doped DWNTs for increasing T_{htt} using $E_{laser}=2.41$ eV laser excitation. Since the laser energy is $E_{laser}=2.41$ eV, we know from the Kataura plot that we are exciting DWNTs whose inner tubes are metallic. Also, increasing the laser excitation energy increases the fourfold splitting of the G′ band, so we select $E_{laser}=2.41$ eV to observe the changes in the four components (G′1 to G′4) of the G′ as T_{htt} is increased. The shaded region marked with an *A* (*B*) corresponds to the G′1 and G′2 (G′3 and G′4) features and is expected to come from the inner (outer) layers of the DWNTs.[31]

A slight increase in the A/B intensity ratio (I_A/I_B) is observed for $T_{htt}=1200-1400$ °C when compared to the pristine sample. Since the D band is still very weak at $T_{htt}\leqslant 1400$ °C, the change in I_A/I_B suggests that the heat treatment anneals possible defects in the inner layer of the DWNT structure and enhances the contribution to the G′ signal from the inner layers (G′1 and G′2).

The correlation between the A/B intensity ratio (I_A/I_B) and the intensity of the RBM peaks from inner layers and the D band can be used to assign the G′1–G′2 (G′3–G′4) features to the inner (outer) layers of our DWNTs. As shown in Fig. 8(d), at $T_{htt}=1400$ °C the intensity ratio I_A/I_B is greater than 1 while at $T_{htt}=1500$ °C, I_A/I_B approaches 1 and at $T_{htt}>1500$ °C $I_A/I_B<1$. At $T_{htt}=1500$ °C, the onset of the decrease in the intensity of the A region (G′1–G′2) exactly

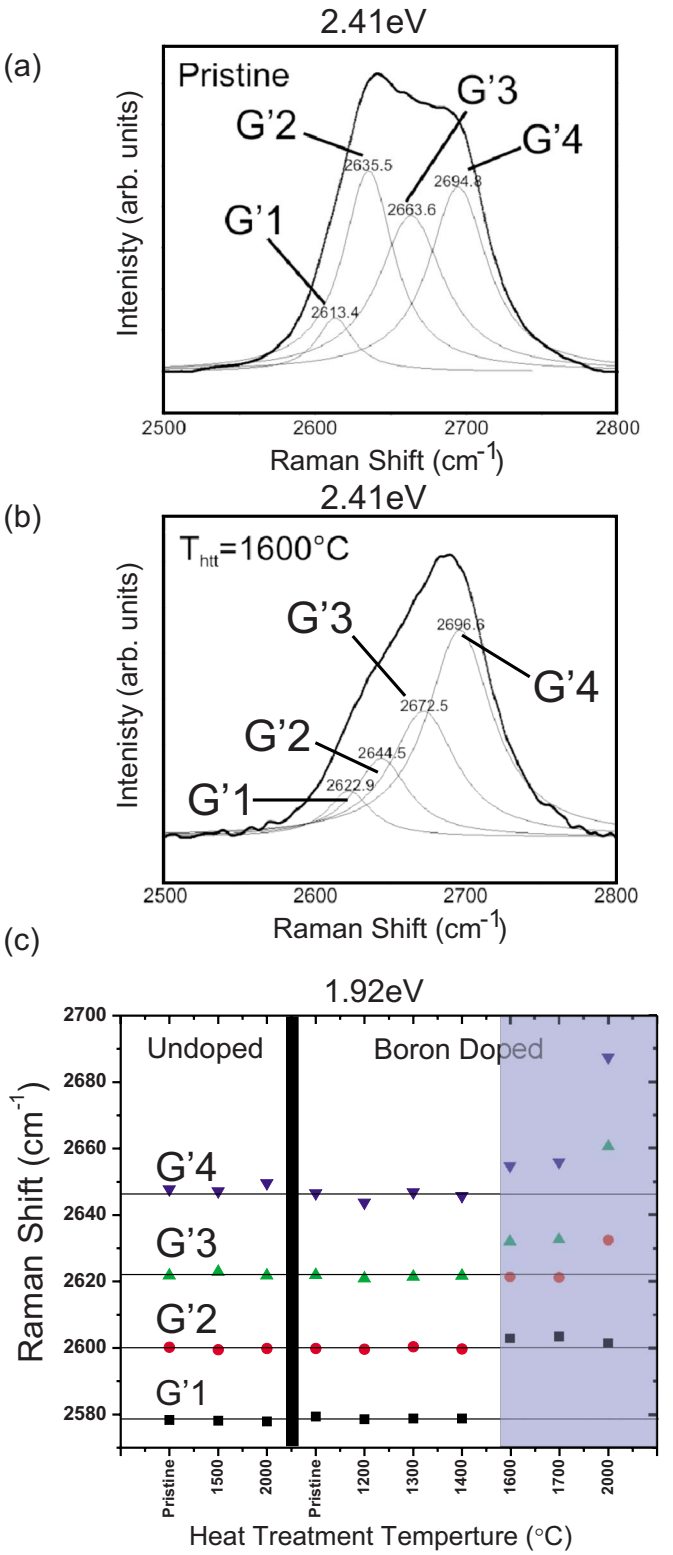

FIG. 9. (Color online) Lineshape analysis for the G′-band region of the Raman spectra at $E_{laser}=2.41$ eV into four components for the cases of (a) pristine (second batch) and (b) heat-treated boron-doped DWNTs at $T_{htt}=1600$ °C (c) A plot of $\omega_{G'}$ for G′1 through G′4 as a function of T_{htt}. All the spectra were taken with $E_{laser}=2.41$ eV which excites DWNTs whose inner tubes are metallic (M). Notice the generalized $\omega_{G'}$ upshift for T_{htt} above 1600 °C.

coincides with the onset of DWNT coalescence,[11] the increase in intensity of the D band and with the onset of the intensity decrease in the RBM peak corresponding to the inner tubes [see $\omega_{RBM} \approx 265$ cm^{-1} in Fig. 3(c)]. This observation allows us to confirm the assignment of G′1–G′2 to the inner layers of the DWNTs that are in resonance with $E_{laser}=2.41$ eV. On the other hand, at $T_{htt}=1500$ °C, the intensity of the B region and the intensity of the RBM peak corresponding to the outer layer [see $\omega_{RBM} \approx 165$ cm^{-1} in Fig. 3(c)] remain unchanged, so we can confirm the assignment of G′3–G′4 to the outer DWNT tubes.

b. Regime II: $T_{htt} > 1500$ °C. In this T_{htt} regime, the required energy for boron-doped DWNT structural destabilization is reached and significant changes occur to the line shape of the G′ band. At $T_{htt}=1600$ °C all the RBM signal is lost, the D band intensity increases considerably [see Fig. 5(a)] and the intensity of the G′3 peak decreases [see Fig. 9(b)]. A similar effect is observed when using $E_{laser}=1.92$ eV. The marked decrease in the intensity of the G′1–G′3 features, the overall broadening of the G′ region, and the generalized loss of a nanotubelike dispersion ($d\omega_{G'}/d_{Elaser}$) all suggest that for $T_{htt} \leqslant 1600$ °C, our sample is mainly composed of a mixture of defective tubular structures and disordered sp^2 carbon materials. Increasing T_{htt} above 1600 °C also results in the alteration of the dispersion of the G′1–G′4 peaks as shown in Fig. 9(c). As presented in Table II, the dispersion of the G′4 feature goes below that of SWNTs (~ 106 cm^{-1}/eV) (Ref. 18) and in fact goes down all the way to 85.4 cm^{-1}/eV. As a reference, at 2.54 eV the G′ for HOPG has two peaks, a weak one at ~ 2690 cm^{-1} and a much higher intensity one at ~ 2740 cm^{-1} that has a dispersion of ~ 99 cm^{-1}/eV.[34]

IV. CONCLUSIONS

We have analyzed the Raman spectra from DWNT bundles that were annealed in the presence and in the absence of elemental boron. An early study of the Raman spectra for such heat treated samples was carried out previously using $E_{laser}=2.33$ eV excitation.[11] In the present work, we observe, in agreement with the earlier study at heat treatment temperatures between 1200 and 2000 °C that the addition of elemental boron both enhances DWNT coalescence and lowers the onset of structural destabilization to $T_{htt}=1500$ °C. In this context, the RBM region of the spectra indicates that smaller diameter tubes disintegrate more readily upon heat treatment than larger diameter tubes, and this disintegration effect is strongly amplified in the boron-doped tubes. Also, we did not detect a difference in the structural destabilization temperature for DWNTs with different metallic and semiconducting configurations. Such a distinction was evaluated using multiple laser excitation energies and different metallic-semiconducting inner/outer tube configurations.

We observe that the D band in DWNT bundles can be fit with two Lorentzians which have their origin in the inner and outer layers of a DWNT as is also observed at the single isolated DWNT level. The overall dependence of the D band intensity on E_{laser} is qualitatively consistent with previous experimental[22] and theoretical[24] reports on nanographite and SWNTs. We find that the I_D/I_G ratio has a power-law dependence on E_{laser} (in the range 1.6–2.41 eV) of the form $I_D/I_G = cE_L^{\alpha}$, where α varies from ~ -2.5 to ~ -3 with decreasing T_{htt} similar to the behavior of graphitic foams.

Both the inner and outer tube constituents of a DWNT contribute to the characteristic line shape of the G band but the semiconducting tubes and the outer tubes have a stronger effect on the overall lineshape. By using various laser lines to excite DWNTs with different configurations, we found that the line shape of the G band is dominated by the outer DWNT layers, regardless of the metallic or semiconducting nature of the inner layers. If the outer tube is metallic, the G band shows a noticeable BWF tail, but if the outer tube is semiconducting, the G^- band is clearly visible. The effect of boron doping is to increase the frequency of the G^+ feature indicating that boron behaves as an acceptor dopant for DWNTs.

Finally, by comparing the intensity of the G′ band to the intensity of the corresponding RBM peaks as a function of heat treatment temperature and as the DWNTs reach coalescence with increasing T_{htt}, we observe that its four components (G′1–G′4) can be assigned to the inner (G′1 and G′2) and the outer tubes (G′3 and G′4) of the DWNTs present in our sample, consistent with but complementary to the behavior of the G′ band in graphene, and consistent with the behavior of the G′ band in individual isolated DWNTs.

ACKNOWLEDGMENTS

The authors gratefully acknowledge financial support from CONACYT Mexico: Grants No. 45762 (M.T.), No. 45772 (M.T.), and No. 41464—Inter American Collaboration (M.T.), Grant No. 42428—Inter American Collaboration (M.T.), the MIT-CONACYT program (M.S.D. M.T.), 2004-01-013/SALUD-CONACYT (M.T.), and PUE-2004-CO2-9 Fondo Mixto de Puebla (M.T.). We also thank CONACYT graduate student grants, Vilore Foods Co., and SEP Mexico for financial support (F.V.P.). The authors M.E., Y.A.K., and T.H. acknowledge support from the CLUSTER project (second stage) and a grant for Specially Promoted Research (Grant No. 19002007) from the Ministry of Education, Culture, Sports, Science and Technology of Japan. The authors F.V.P., H.S., G.G.S., S.G.C., and M.S.D. gratefully acknowledge support from NSF/DMR under Grant No. 07-04197. We are grateful to H. Farhat, A. Reina, D. Nezich, M. Hofmann, J. Campos, E. Barros, A. G. Souza, and L. G. Cancado for helpful discussions.

[1] R. Saito, G. Dresslhaus, and M. S. Dresselhaus, *Physical Properties of Carbon Nanotubes* (Imperial College, London, 1998).
[2] G. Chen, S. Bandow, E. R. Margine, C. Nisoli, A. N. Kolmogorov, V. H. Crespi, R. Gupta, G. U. Sumanasekera, S. Iijima, and P. C. Eklund, Phys. Rev. Lett. **90**, 257403 (2003).
[3] Y. A. Kim, H. Muramatsu, T. Hayashi, M. Endo, M. Terrones, and M. S. Dresselhaus, Chem. Phys. Lett. **398**, 87 (2004).
[4] W. A. de Heer, A. Châtelain, and D. Ugarte, Science **270**, 1179 (1995).
[5] M. Endo, H. Muramatsu, T. Hayashi, Y. A. Kim, M. Terrones, and N. S. Dresselhaus, Nature (London) **433**, 476 (2005).
[6] S. Bandow, M. Takizawa, K. Hirahara, M. Yudasaka, and S. Iijima, Chem. Phys. Lett. **337**, 48 (2001).
[7] W. Z. Li, J. G. Wen, M. Sennett, and Z. F. Ren, Chem. Phys. Lett. **368**, 299 (2003).
[8] J. F. Colomer, L. Henrard, E. Flahaut, G. V. Tendeloo, A. A. Lucas, and P. Lambin, Nano Lett. **3**, 685 (2003).
[9] A. Jorio, G. Dresselhaus, and M. S. Dresselhaus, *Carbon Nanotubes: Advanced Topics in the Synthesis, Structure, Properties, and Applications* (Springer, Germany, 2007), Chap. 16, p. 495.
[10] E. Flahaut, R. Bacsa, A. Peigney, and C. Laurent, Chem. Commun. (Cambridge) **2003**, 1442.
[11] M. Endo, Y. A. Kim, T. Hayashi, H. Muramatsu, M. Terrones, R. Saito, F. Villalpando-Paez, S. G. Chou, and M. S. Dresselhaus, Small **2**, 1031 (2006).
[12] F. Villalpando-Paez, D. N. H. Son, Y. P. Hsieh, J. Kong, Y. A. Kim, D. Shimamoto, H. Muramatsu, T. Hayashi, M. Endo, M. Terrones, and M. S. Dresselhaus, Nano Lett. **8**, 3879 (2008).
[13] Y. A. Kim, H. Muramatsu, T. Hayashi, M. Endo, M. Terrones, and M. S. Dresselhaus, Chem. Vap. Deposition **12**, 327 (2006).
[14] Y.-A. Kim, H. Muramatsu, M. Kojima, T. Hayashi, M. Endo, M. Terrones, and M. S. Dresselhaus, Chem. Phys. Lett. **420**, 377 (2006).
[15] G. G. Samsonidze, R. Saito, N. Kobayashi, A. Gruneis, J. Jiang, A. Jorio, S. G. Chou, G. Dresselhaus, and M. S. Dresselhaus, Appl. Phys. Lett. **85**, 5703 (2004).
[16] V. N. Popov, New J. Phys. **6**, 17 (2004).
[17] A. Jorio, C. Fantini, M. A. Pimenta, R. B. Capaz, G. G. Samsonidze, G. Dresselhaus, M. S. Dresselhaus, J. Jiang, N. Kobayashi, A. Gruneis, and R. Saito, Phys. Rev. B **71**, 075401 (2005).
[18] M. S. Dresselhaus, G. Dresselhaus, R. Saito, and A. Jorio, Phys. Rep. **409**, 47 (2005).
[19] A. G. Souza Filho, M. Endo, H. Muramatsu, T. Hayashi, Y. A. Kim, E. B. Barros, N. Akuzawa, G. G. Samsonidze, R. Saito, and M. S. Dresselhaus, Phys. Rev. B **73**, 235413 (2006).
[20] F. Villalpando-Paez, M.S. thesis, MIT, 2006.
[21] E. B. Barros, N. S. Demir, A. G. Souza Filho, J. M. Filho, A. Jorio, G. Dresselhaus, and M. S. Dresselhaus, Phys. Rev. B **71**, 165422 (2005).
[22] L. G. Cancado, K. Takai, T. Enoki, M. Endo, Y. A. Kim, H. Mizusaki, A. Jorio, L. N. Coelho, R. Magalhaes-Paniago, and M. A. Pimenta, Appl. Phys. Lett. **88**, 163106 (2006).
[23] M. A. Pimenta, G. Dresselhaus, M. S. Dresselhaus, L. G. Cancado, A. Jorio, and R. Saito, Phys. Chem. Chem. Phys. **9**, 1276 (2007).
[24] K. Sato, R. Saito, Y. Oyama, J. Jiang, L. G. Cancado, M. A. Pimenta, A. Jorio, G. G. Samsonidze, G. Dresselhaus, and M. S. Dresselhaus, Chem. Phys. Lett. **427**, 117 (2006).
[25] P. L. Gai, O. Stephan, K. McGuire, A. M. Rao, M. S. Dresselhaus, G. Dresselhaus, and C. Colliex, J. Mater. Chem. **14**, 669 (2004).
[26] M. A. Pimenta, A. Jorio, S. D. M. Brown, A. G. Souza, G. Dresselhaus, J. H. Hafner, C. M. Lieber, R. Saito, and M. S. Dresselhaus, Phys. Rev. B **64**, 041401 (2001).
[27] S. Piscanec, M. Lazzeri, J. Robertson, A. C. Ferrari, and F. Mauri, Phys. Rev. B **75**, 035427 (2007).
[28] M. Paillet, T. Michel, J. C. Meyer, V. N. Popov, L. Henrard, S. Roth, and J.-L. Sauvajol, Phys. Rev. Lett. **96**, 257401 (2006).
[29] Q. H. Yang, P. X. Hou, M. Unno, S. Yamauchi, R. Saito, and T. Kyotani, Nano Lett. **5**, 2465 (2005).
[30] A. C. Ferrari, J. C. Meyer, V. Scardaci, C. Casiraghi, M. Lazzeri, F. Mauri, S. Piscanec, D. Jiang, K. S. Novoselov, S. Roth, and A. K. Geim, Phys. Rev. Lett. **97**, 187401 (2006).
[31] E. B. Barros, H. Son, G. G. Samsonidze, A. G. Souza Filho, R. Saito, Y. A. Kim, H. Muramatsu, T. Hayashi, M. Endo, J. Kong, and M. S. Dresselhaus, Phys. Rev. B **76**, 045425 (2007).
[32] W. Ren and H. M. Cheng, in *Nanoscale Phenomena Basic Science to Device Applications*, Lecture Notes in Nanoscale Science and Technology Vol. 2 (Springer, New York, 2007), Chap. 4, pp. 29–39.
[33] A. G. Souza Filho, A. Jorio, G. G. Samsonidze, G. Dresselhaus, M. A. Pimenta, M. S. Dresselhaus, A. K. Swan, M. S. Unlu, B. B. Goldberg, and R. Saito, Phys. Rev. B **67**, 035427 (2003).
[34] T. Shimada, T. Sugai, C. Fantini, M. Souza, L. G. Cancado, A. Jorio, M. A. Pimenta, R. Saito, A. Grüneis, G. Dresselhaus, M. S. Dresselhaus, Y. Ohno, T. Mizutani, and H. Shinohara, Carbon **43**, 1049 (2005).